JOURNAL OF PROPULSION AND POWER
Vol. 33, No. 4, July–August 2017

Design Procedure of a Movable Pintle Injector for Liquid Rocket Engines

Min Son,* Kanmaniraja Radhakrishnan,† and Jaye Koo‡
Korea Aerospace University, Goyang, Gyeonggi-do 10540, Republic of Korea
Oh Chae Kwon§
Sungkyunkwan University, Suwon, Gyeonggi-do 16419, Republic of Korea
and
Heuy Dong Kim§
Andong National University, Andong, Gyeongsangbuk-do 36729, Republic of Korea

DOI: 10.2514/1.B36301

Variable-area injectors are suitable choices for developing throttleable rocket engines because it is difficult to efficiently control thrust when fixed-area injectors are used. A pintle injector is a variable-area injector that can control the mass flow rate of propellants, thereby replacing a large injector plate having several injector elements with a single injector unit. To achieve proper performance under all throttling conditions, a design procedure was established for a pintle injector based on spray characteristics. The spray angle and Sauter mean diameter of the droplets were critical performance parameters. In spray experiments using water and air as simulants under atmospheric conditions, backlight imaging and laser-diffraction methods were used to measure the spray angle and Sauter mean diameter. The velocity ratio, nondimensionalized opening distance, and Weber number were considered as major nondimensional numbers. Empirical correlations were formulated between performance parameters and nondimensional numbers; these correlations were applied to the design procedure herein. Consequently, a 500 N combustor with a pintle injector was designed using this procedure. A control plan for the pintle-opening distance under lower throttling conditions was also obtained for designing a small combustor. Furthermore, the most sensitive parameters in the injector geometry were confirmed via sensitivity analysis.

Nomenclature

A_c	=	cross-sectional area of combustion chamber
A_{cg}	=	center gap area
A_{min}	=	minimum orifice area near pintle tip
B	=	transfer number for droplet vaporization
c_p	=	specific heat capacity at constant pressure
D_c	=	cylinder chamber diameter
D_{cg}	=	center gap diameter
D_{post}	=	post diameter
D_{pr}	=	pintle rod diameter
D_{pt}	=	pintle tip diameter
D_{32}	=	Sauter mean diameter
K	=	characteristic parameter for spray angle
k	=	thermal conductivity of hot gas
L_c	=	cylinder chamber length
L_{min}	=	minimum opening near pintle tip
L_{open}	=	pintle-opening distance
$\dot{m}$	=	mass flow rate
P	=	pressure
Pr	=	Prandtl number
p	=	variable for spray angle correlation
q	=	variable for Sauter mean diameter correlation
R_{post}	=	radius of pintle post
r_{post}	=	post recess length
S	=	drag coefficient for vaporization model
s	=	variable for spray angle correlation
T	=	temperature
t_{ann}	=	annular gap thickness
t_{post}	=	post thickness
t_{pt}	=	pintle tip thickness
t^*	=	vaporization time
u_{d0}	=	initial droplet velocity
V	=	injection velocity
We	=	Weber number
x^*	=	actual vaporization distance
α	=	spray half-angle
β	=	variable for surface tension
Γ	=	variable for droplet vaporization
ξ	=	nondimensional pintle tip angle
θ_{post}	=	post angle
θ_{pt}	=	pintle tip angle
ρ	=	density
σ	=	surface tension

Subscripts

b	=	boiling
c	=	combustion gas property
cr	=	critical
gas	=	gas propellant
liq	=	liquid propellant
max	=	maximum
r	=	reduced

Presented as Paper 2016-1453 at The AIAA Science and Technology Forum and Exposition, San Diego, CA, 4–8 January 2016; received 26 April 2016; revision received 6 September 2016; accepted for publication 19 September 2016; published online 19 December 2016.

*Ph.D. Student, Department of Aerospace and Mechanical Engineering. Student Member AIAA.
†Graduate Student, Department of Aerospace and Mechanical Engineering.
‡Professor, School of Aerospace and Mechanical Engineering; jykoo@kau.ac.kr. Senior Member AIAA.
§Professor, School of Mechanical Engineering. Senior Member AIAA.

I. Introduction

A PINTLE injector is a type of variable-area injector that was developed in the 1950s for application to throttleable liquid rocket engines; it served as the main injector in the Apollo mission's lunar module [1–3]. Although this variable-area injector was developed in the early space era, fixed-area injectors such as the shear coaxial injectors and coaxial swirl injectors have mainly been used

until recently. However, variable-area injectors, especially pintle injectors, have recently attracted renewed attention as next-generation injectors because of their associated benefits compared with relatively newer engines. Previous studies were conducted by TRW, Inc., the predecessor of Northrop Grumman Space Technology. Nevertheless, several results of their research were not disclosed [4–7]. Throttleable low-cost engines have been recently developed; a means to maintain optimized injection conditions at all thrust levels is required because conventional injectors with fixed areas have relatively poor efficiencies at lower thrust levels. A pintle injector can control both the injection area and velocity to maintain good spray conditions at low rates of propellant flow. Moreover, one pintle injector can cover the entire combustion chamber because it has a wide spray angle. This allows heavy injector plates comprising several injector elements to be replaced by one pintle-injector unit, thereby reducing manufacturing costs. Researchers at SpaceX have demonstrated pintle injectors in their Grasshopper and Merlin rockets [8] and proved that they have the potential to become the preferred injectors in the future.

Many research groups in universities have attempted to develop pintle-injector engines, however, only injection conditions have been changed without design studies. Austin and Heister investigated the combustion performance of a hole-injection-type pintle injector under variance of major parameters, such as the total momentum ratio and the characteristic length of the chamber [9]. They concluded that the optimal characteristic length was greater than 30 in. and that a total momentum ratio of 0.7 was suitable for a 1.7-in.-diam chamber. They suggested some interesting parameters affecting combustion performance; however, the effects of injector geometries were not considered. Bedard et al. built a Lox-centered pintle injector and improved its annular design to achieve uniform injection [10]. Yue et al. investigated numerical simulation of the pintle-injector combustor using unsymmetrical dimethylhydrazine and N_2O4 and revealed two recirculation areas in the chamber [11]. Sakaki et al. studied a pintle injector using ethanol and liquid oxygen. They conducted an experimental study of the planar pintle injector (which was a simplified axisymmetric pintle injector) and they visualized chemiluminescence of CH [12]. Using the same method in a planar study, the axisymmetric injector was also investigated. Instability and lower combustion efficiency were observed at lower total momentum ratio (TMR) conditions [13].

Despite the many advantages of the pintle injector, they are difficult to design because of their numerous design parameters and moving mechanisms. Thus, it is important to consolidate the various design parameters down to just a few and evaluate them to yield maximum performance. Furthermore, to maintain maximum performance under all throttling conditions, the pintle operation must be optimized. Nevertheless, recent research has not arrived at a general design for a pintle injector and specific parametric studies for optimal design have not been conducted. Thus, we have suggested a simplified design for a movable pintle injector and have tried to find effective nondimensional parameters. In our first study, the total momentum ratio and Weber number were considered and determined to change the spray angle [14] and Sauter mean diameter (SMD) [15]. In the studies that followed, the transition of the minimum area inside the pintle flowpath was revealed, which was a special characteristic of the movable pintle injector [16]. Finally, in this study, an additional spray experiment has been conducted to find effects of pintle tip angles upon spray performances, and performance correlations were experimentally obtained under various injection conditions. Using these experimental results, a design procedure was introduced to achieve optimized operation.

II. Experimental Results and Empirical Correlations

A. Concept of a Pintle Injector

As illustrated in Fig. 1, a pintle injector has a simple design that targets a combination of liquid–gaseous propellants such as liquid oxygen and gaseous methane. A moving pintle at the center controls the liquid propellant and an annular gap on the outside of the inner body injects the gaseous propellant without any area control.

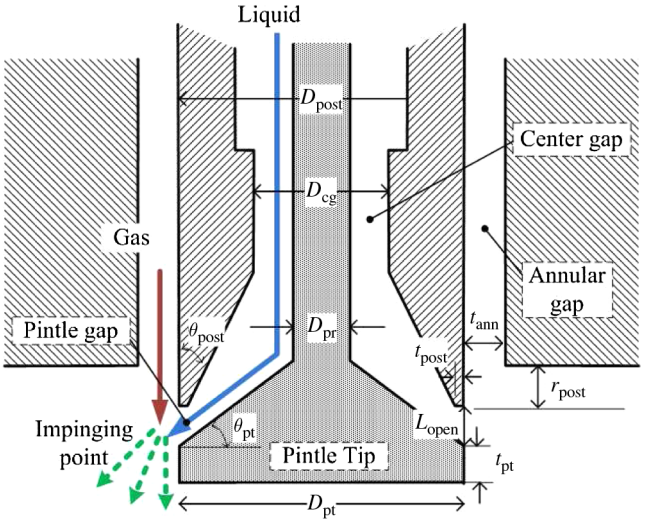

Fig. 1 Schematic of the pintle injector.

Propellants from the center and annular nozzles collide near the pintle tip. The dimensions are detailed in Table 1. In this study, three types of pintle tips with different tip angles were used and the post angle was fixed at 30.0 deg. Because the post angle was sufficiently small, the minimum orifice area in the pintle nozzle was always determined at the post tip. Because of the variable area of the pintle nozzle, the discharge coefficient could also change with the minimum orifice area in the pintle nozzle. The minimum orifice area shown in Fig. 2 was estimated and geometrically calculated according to Eq. (1):

$$A_{\min} = \frac{\pi}{\sin\theta_{pt}}\left[(R_{post} - t_{post})^2 - (R_{post} - t_{post} - L_{open}\sin\theta_{pt}\cos\theta_{pt})^2\right] \quad (1)$$

In Fig. 2a, the minimum opening distance L_{min} was defined using the perpendicular line from the post tip to pintle tip slope. As shown in Fig. 2b, the area A_{min} from the zero-opening distance was the minimum area inside the pintle nozzle. However, A_{min} was the same at a specific point as the center gap area A_{cg}, which was the constant area determined by the initial pintle design. After this transition point, the minimum area inside the pintle nozzle changed to the center gap area and could not be changed as the pintle-opening distance increased. As shown in Fig. 3 and Table 2, different pintle tip angles resulted in different transition points and these transition points increased with increasing pintle tip angle. The transition point of the minimum area was a special characteristic of the variable-area injector and reflecting this in the design criteria was necessary. In the figure, the spray experiment indicated a nonzero minimum opening distance. The uniform liquid sheet was not constructed within 0.1 mm of the opening distance. Consequently, the experimental condition of the opening distance was controlled from 0.2 mm at a 0.1 mm interval.

Table 1 Dimensions of the pintle injector and experimental conditions

Parameter	Value
Post diameter D_{post}, mm	8.0
Center gap diameter D_{cg}, mm	4.55
Pintle rod diameter D_{pr}, mm	3.0
Pintle tip diameter D_{pt}, mm	8.0
Annular gap thickness t_{ann}, mm	0.50
Post angle θ_{post}, deg	30
Pintle tip angle θ_{pt}, deg	0, 20, 40
Pintle tip thickness t_{pt}, mm	1.0
Post recess length r_{post}, mm	3.0
Post thickness t_{post}, mm	0.5
Pintle-opening distance L_{open}, mm	0.2–1.0

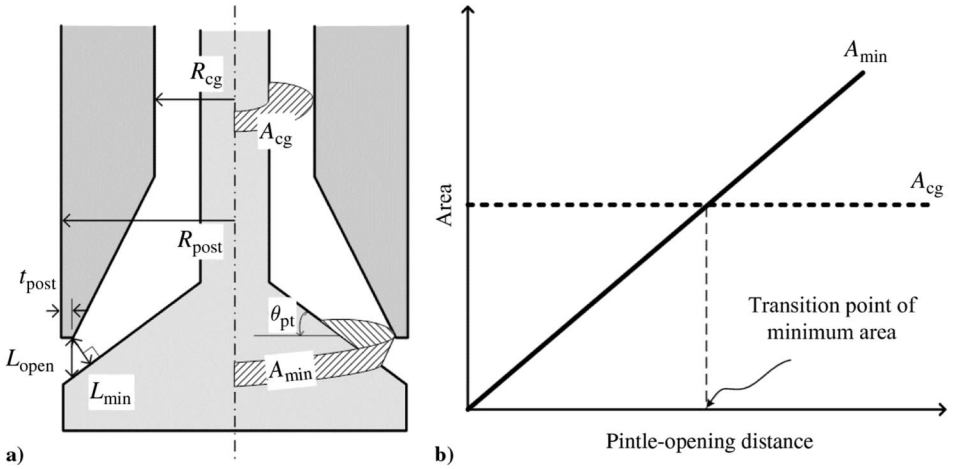

Fig. 2 Remarkable dimensions inside the pintle nozzle for the minimum-area transition: a) schematic and b) definition of a transition point.

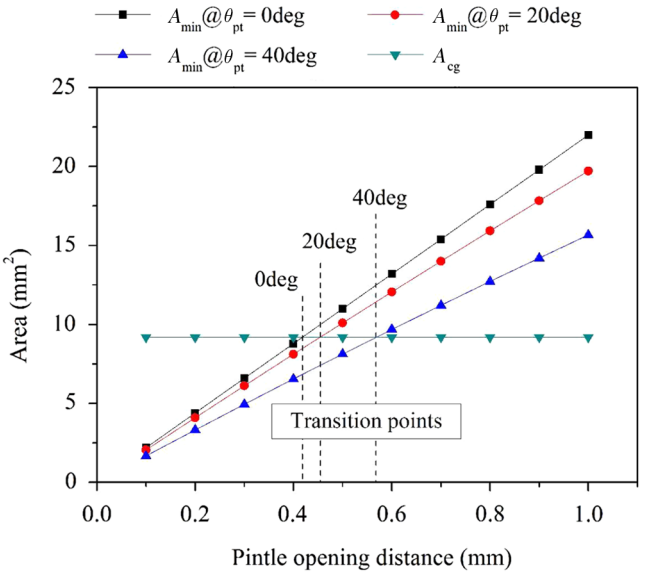

Fig. 3 Minimum orifice area near the pintle tip according to pintle-opening distance and transition points.

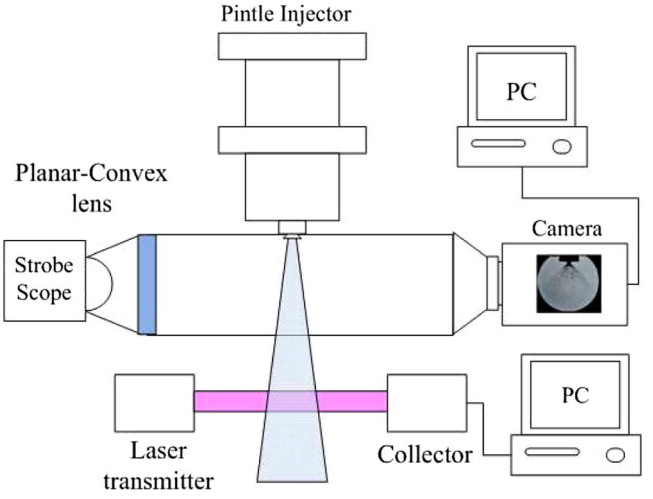

Fig. 4 Schematic of the experimental system.

B. Experimental Apparatus and Methods

The two major variables in a pintle injector are the spray angle and atomization performance. As the element unit injects all propellants, fast mixing and a wide spray surface are necessary to quickly burn them. Therefore, a wide spray angle should be used to exploit the wide chamber area. Generally, the combustion efficiency and burning rate of the liquid fuel are related to atomization characteristics that are represented by the droplet diameter. Hence, the spray angle and SMD of the droplets were selected as the major design variables in this study. An atmospheric spray experiment was conducted using water and air as simulants of real propellants to determine optimal nondimensional variables for the procedure. For precision pintle control, a micrometer with a 0.001 mm interval was used and connected to the pintle rod using a rigid motor coupler.

Table 2 Transition point due to different pintle tip angles

Pintle tip angle, deg	Estimated transition point of opening distance, mm
0	0.418
20	0.454
40	0.568

Figure 4 shows the entire experimental setup for capturing spray images and measuring SMDs. A stroboscope was used as the light source, and planar-convex lenses were used to generate parallel light rays. Spray images were captured using a high-resolution complementary metal-oxide semiconductor camera with a resolution of 4256 × 2832 pixels and a 1 s exposure time. The density–gradient–magnitude (DRM) images were obtained by processing the spray images. In a previous study [14], the spray angle was defined from the center of the injector. However, the new spray angle is defined as shown in Fig. 5. Spray angles were defined from the post tip (i.e., the theoretical impinging point) and a distance of 50 mm as measured using the DRM images. A laser-diffraction meter was used to measure the SMDs based on laser-diffraction theory, which is in turn based on Mie scattering. The SMDs were also measured at the same axial point as the spray angle measurement. The volume-averaged SMDs were measured using the diffraction meter. Sprays penetrated the thick laser and the analyzer calculated the distribution and averaged diameter using the diffracted signal. The laser diameter was 29.5 mm with a 632.8 nm wavelength.

C. Experimental Results

As mentioned in the previous section, the pintle injector has the special characteristic of a variable nozzle area. Along with the variable nozzle area, the flow characteristic is dependent on the pintle-opening distance. The hypothesis of the minimum area transition in Fig. 2 is similar to the actual transition that was observed as shown in Fig. 6a. At the transition point, there was a sudden change in the spray characteristics of the experiment. Additionally, the actual transition point was not fixed with uncertainties because of the flow

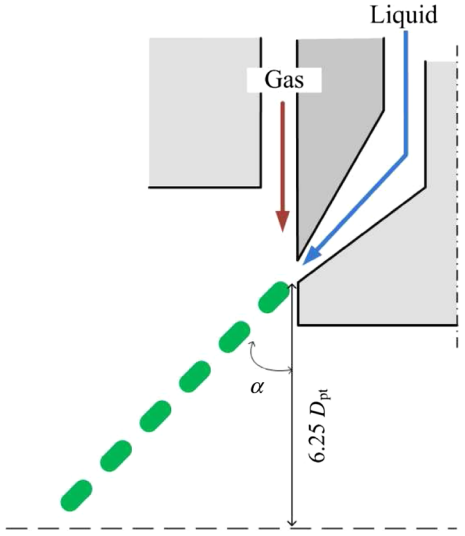

Fig. 5 Definition of the spray angle.

conditions within the pintle nozzle (e.g., flattering of a liquid sheet). Therefore, from the combustion viewpoint, this transition could cause unexpected instability and a controllable range of the opening distance should be considered below the transition point. The transition points can be estimated by Eq. (2), where A_{cg} is used instead of A_{min} as in Eq. (1), and the opening distance could be considered as the maximum opening distance. According to Eq. (2), the maximum opening distances could be changed because of the pintle tip angles. The estimated transition points determined by Eq. (2) corresponded to the bending points of Fig. 6a:

$$L_{open,max} = \frac{R_{post} - \sqrt{R_{post}^2 - A_{cg}(\sin\theta_{pt}/\pi)}}{\sin\theta_{pt}\cos\theta_{pt}} \tag{2}$$

The ideal mass flow rates could be calculated using the measured pressure drops through the pintle nozzle and from the definition of the minimum area within the pintle nozzle. Using these rates, the discharge coefficients were calculated as Eq. (3). Before the transition point, the minimum orifice area near the pintle could mainly affect the pressure drop of the injector, whereas the center gap area could control the pressure drop after the transition point. As shown in Fig. 6b, the discharge coefficients of A_{min} were higher than those of A_{cg} before the transition point. After the transition point, these trends were reversed and the coefficients of A_{cg} were almost constant despite the increasing opening distance because the flow was choked in the center gap area:

$$\begin{cases} C_d = \dfrac{\dot{m}_{liq}}{A_{min}\sqrt{2\rho_{liq}\Delta P_{liq}}} & A_{cg} \geq A_{min} \\ C_d = \dfrac{\dot{m}_{liq}}{A_{cg}\sqrt{2\rho_{liq}\Delta P_{liq}}} & A_{cg} < A_{min} \end{cases} \tag{3}$$

$$TMR = \frac{\dot{m}_{liq}V_{liq}\cos\theta_{pt}}{\dot{m}_{gas}V_{gas} + \dot{m}_{liq}V_{liq}\sin\theta_{pt}} \tag{4}$$

$$We = \frac{(\rho_{gas})(L_{open})(V_{gas} - V_{liq})^2}{\sigma_{liq}} \tag{5}$$

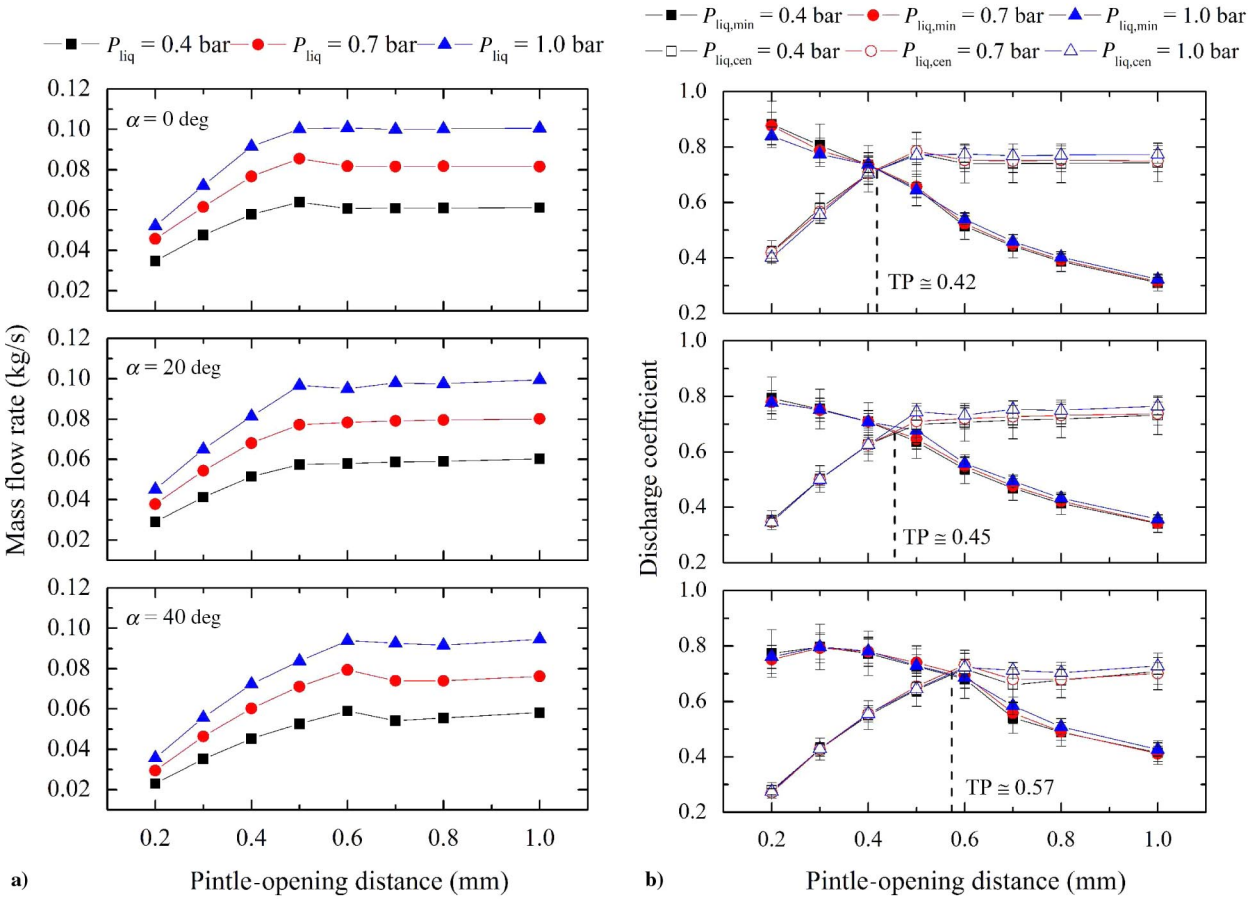

Fig. 6 Flow characteristics of a pintle nozzle: a) mass flow rate and b) discharge coefficient.

$$\sigma_{\text{liq}} = (T_{\text{cr}}P_{\text{cr}}^2)^{1/3}(0.133\beta - 0.28)(1 - T_r)^{11/9} \tag{6}$$

where

$$\beta = 0.91\left(1 + \frac{T_{rb}\,\ell n\, P_{\text{cr}}}{1 - T_{rb}}\right) T_r = \frac{T_{\text{liq}}}{T_{\text{cr}}} T_{br} = \frac{T_b}{T_{\text{cr}}}$$

The Weber numbers and TMRs of the spray experiments are indicated in Fig. 7a. The TMR can be defined as shown in Eq. (4) and denotes the ratio between radial and axial momenta. The aerodynamic Weber number was used for correlation of the SMD, and the bulk velocities were also used regardless of the injection direction. The surface tension in the Weber number was calculated by the empirical equation suggested in [17–19], as shown in Eq. (6). In this equation, the units of surface tension and pressure are dyne per meter and standard atmosphere, respectively. The experiment was conducted up to a Weber number of approximately 4500 and a TMR of approximately 0.9. As shown in Fig. 7b, spray angles and SMDs had a linear relation and SMDs decreased along with the spray angle as well as the pintle tip angle.

D. Empirical Correlations

To generalize spray characteristics, nondimensional parameters, as calculated by Eqs. (5) and (7), were adopted. The first one is Weber number and K is the special characteristic parameter for the correlation of the spray angle as in Eq. (7). It contains the velocity ratio and nondimensionalized opening distance. K can also be expressed as a product of the mass flow rate ratio, density ratio, and certain dimensions of the injector, such as the pintle tip diameter and annular gap thickness. In this equation, the velocities refer to those of bulk injection and the liquid velocity was calculated using the area based on L_{open}, rather than L_{min}. Densities were calculated under atmospheric conditions:

$$K = \frac{V_{\text{gas}}}{V_{\text{liq}}}\frac{t_{\text{ann}}}{L_{\text{open}}} = \frac{\dot{m}_{\text{gas}}}{\dot{m}_{\text{liq}}}\frac{\rho_{\text{liq}}}{\rho_{\text{gas}}}\left(\frac{D_{\text{pt}}}{D_{\text{pt}} + t_{\text{ann}}}\right) \tag{7}$$

To determine the types of correlation functions for spray characteristics, physical limitations were considered. As shown in Fig. 8a, the spray angle initially had a clear upper limit when the gas-injection velocity was equal to zero. The liquid sheet generated a constant spray angle because of the pintle tip angle. However, the spray angle could be appropriately changed by the opening distance and ratio of the gas–liquid injection velocities. As the gas-injection velocity increased, the spray angle decreased down to a specific lower limit. Thus, a logistic function was used for the correlation of the spray angles. In contrast, the SMD only approached a lower limit as the gas-injection velocity increased, as shown in Fig. 8b. This was because the SMD of the unbroken liquid sheets without gas injection could be expressed as infinity. Accordingly, a power function was suitable to formulate the relation between SMD and Weber number. These empirical trends are illustrated as shown in Fig. 9. The spray angle has upper and lower limits, whereas the SMD only has a lower limit.

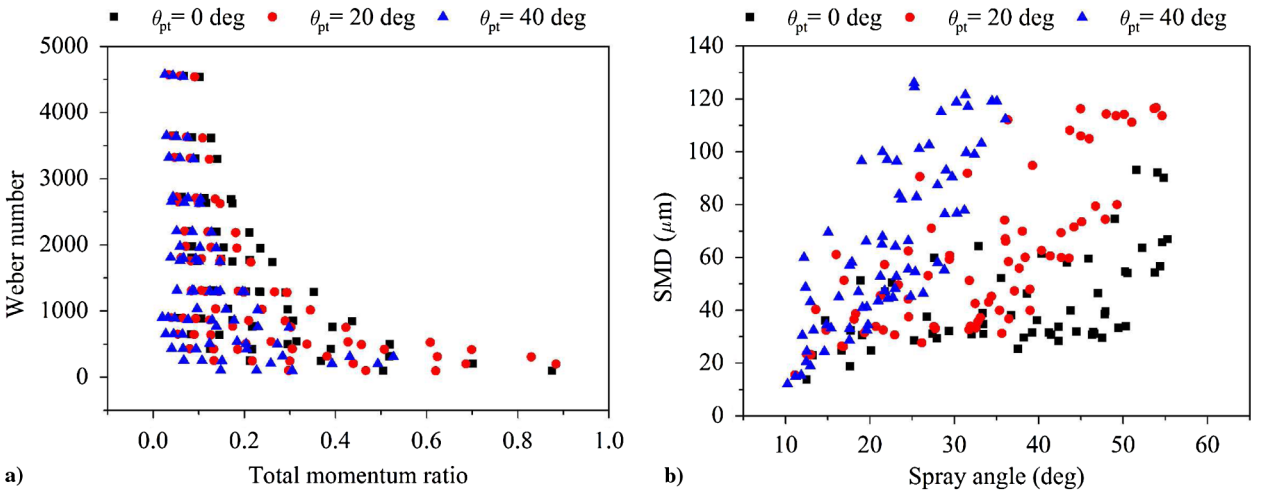

Fig. 7 Results of a) spray angle and b) SMD.

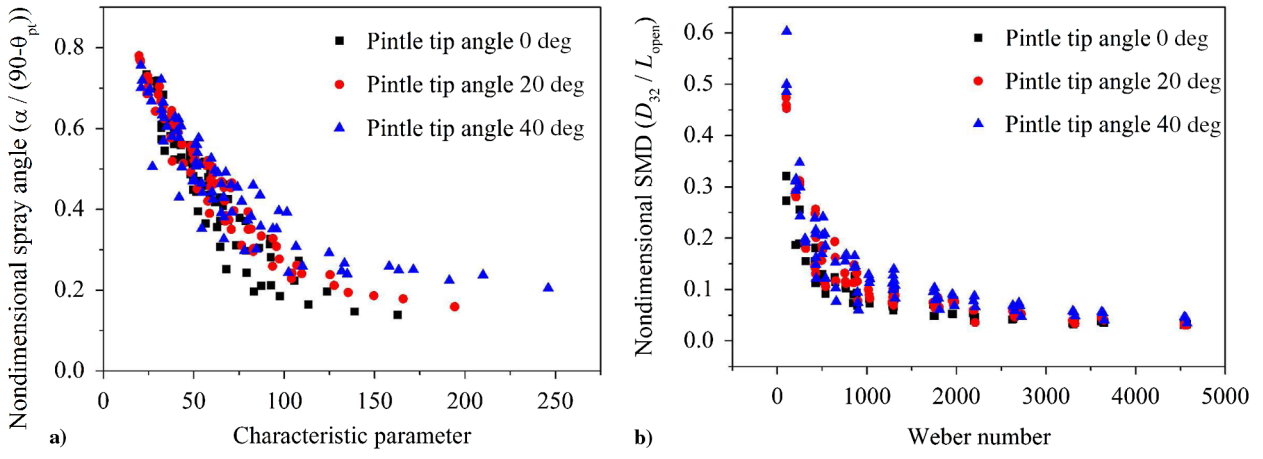

Fig. 8 Experimental results according to nondimensional numbers: a) spray angle and b) SMD.

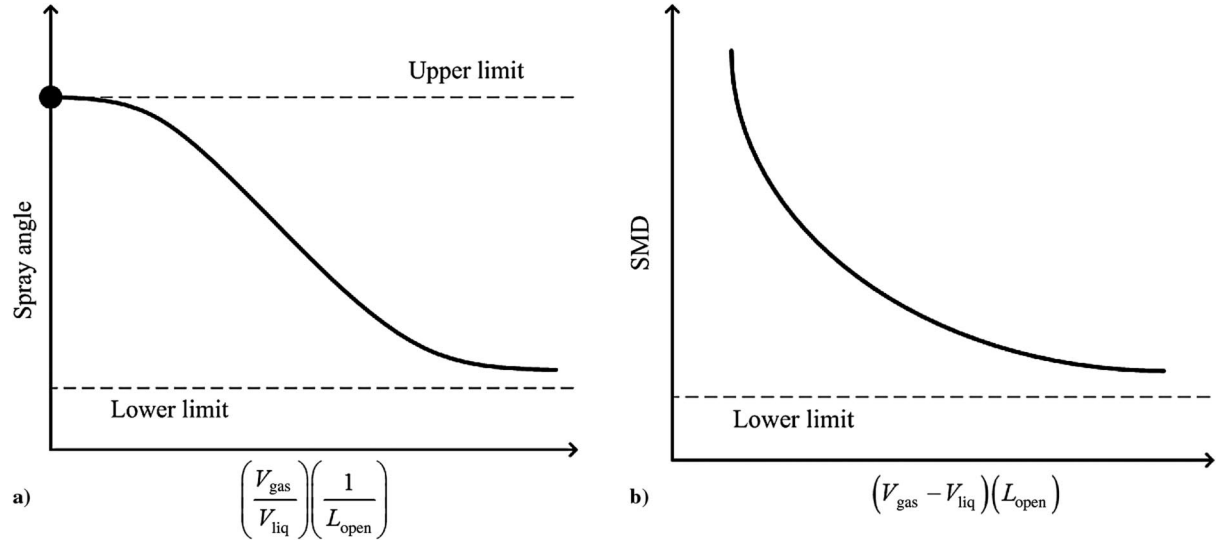

Fig. 9 Physical limitations of spray characteristics; a) spray angle and b) SMD.

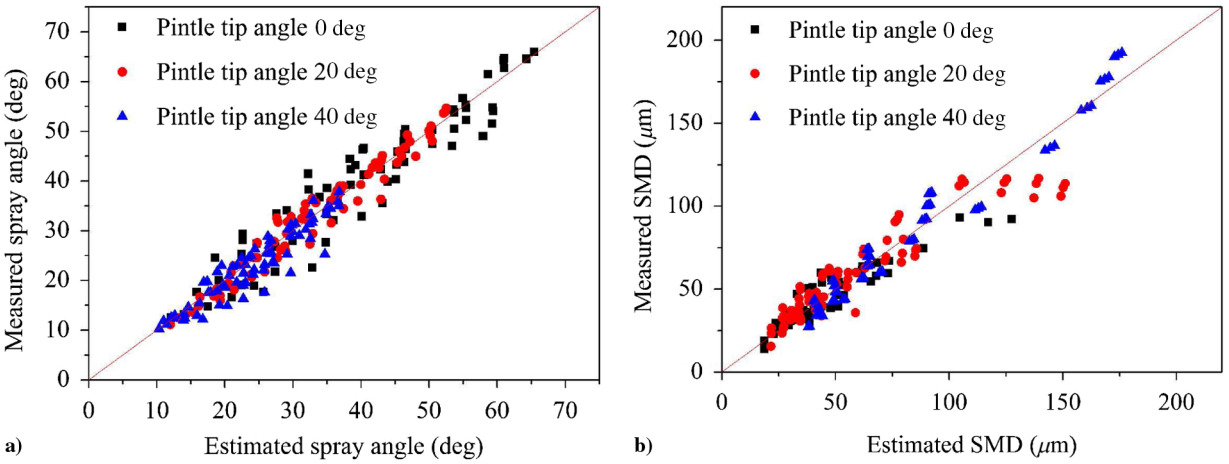

Fig. 10 Comparison of the measured and estimated spray characteristics: a) spray angle and b) SMD.

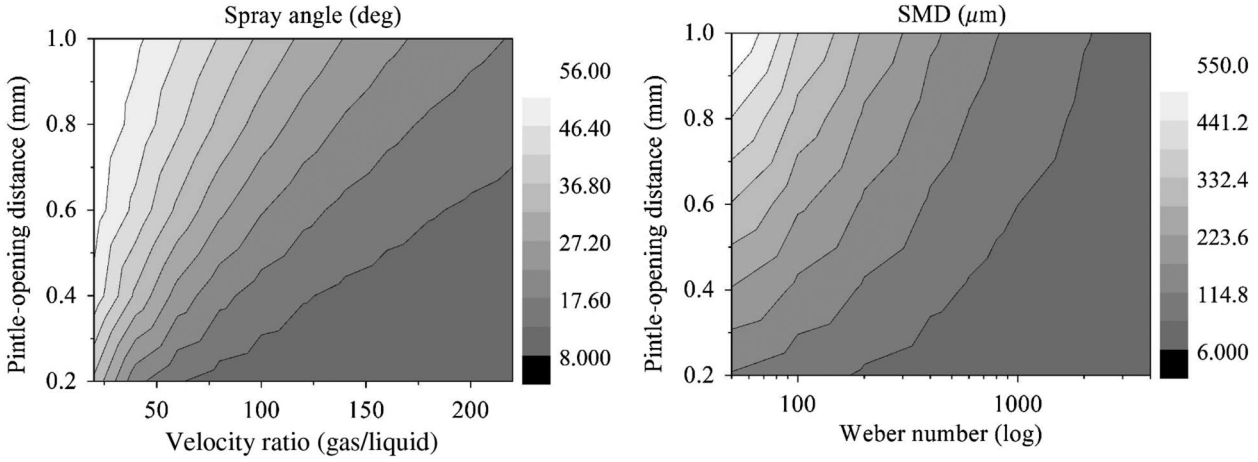

Fig. 11 Contours of a) spray angles and b) SMDs due to major parameters.

Finally, correlations were obtained to estimate the spray angles and SMDs by Eqs. (8) and (9). In addition to K and We, these equations contain the pintle tip angle in nondimensionalized form. In Eq. (9), the units of SMD and opening distance are micrometer and millimeter, respectively. As shown in Fig. 10, the estimated spray angle and SMD reasonably track the measured values. The coefficient of determination (R^2) was 0.912 for spray angle correlation and the global uncertainty was ± 6.46 at a confidence

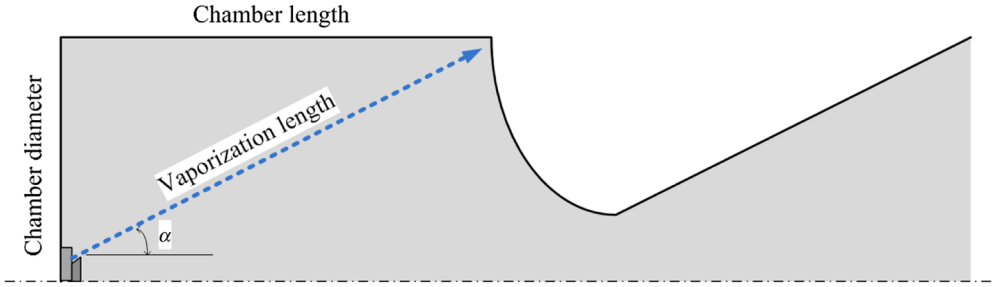

Fig. 12 Schematic of vaporization distance in the combustor.

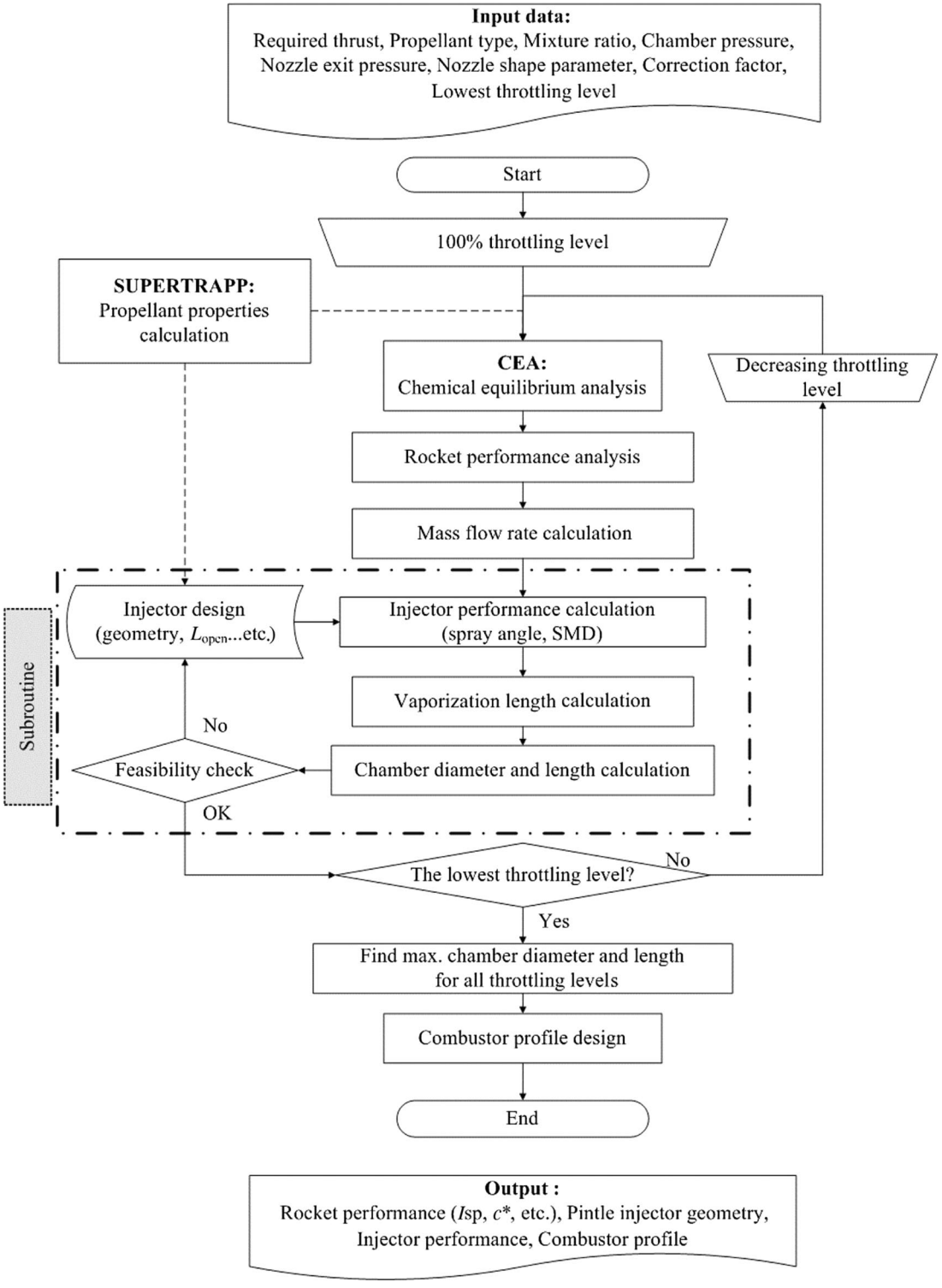

Fig. 13 Flowchart of combustor design procedure including the injector design subroutine.

level 95%. R^2 was 0.871 with an uncertainty of ±26.27 at the same confidence level as that for the SMD correlation:

$$\alpha = 90(\xi)\exp\left[\frac{s-0.2}{1+(K/90)^p} - s\right] \tag{8}$$

where

$$\xi = \frac{90-\theta_{\text{pt}}}{90}, \qquad s = 1.15 + 1.35\xi, \qquad p = 1.30 + 0.90\xi$$

$$D_{32} = 10^3(L_{\text{open}})(\xi^{-1})\exp[4.0 - q(We^{0.1})] \tag{9}$$

where

$$\xi = \frac{90-\theta_{\text{pt}}}{90}, \qquad q = 3.455\text{–}0.225\xi$$

As shown in Fig. 11, the global trends of the spray characteristics were illustrated by contours due to major parameters such as velocity ratio, Weber number, and opening distance. The spray angle was proportional to the opening distance and inversely proportional to the velocity ratio. The SMD was also proportional to the opening distance and inversely proportional to the logarithmic Weber number.

III. Design Procedure and Results

A. Design Procedure and Methods

The spray angles and SMDs could be used to design the combustion chamber. It is necessary to complete the reaction of propellants in the combustion chamber before the propellants reach the nozzle throat to ensure higher combustion efficiency. In this study, the burning region was restricted to the cylindrical part of the combustor, thus the reaction had to be completed in the cylindrical chamber. It was assumed that the end of vaporization indicated the end of combustion because the vaporization process is slower than the chemical reaction of the diffusion flames.

As shown in Fig. 12, the pintle injector constructs a wide spray and the optimized chamber size could be determined by the propellants' vaporization distances. The vaporization distance and time of the droplets could be calculated by simple equilibrium or nonequilibrium models. An equilibrium model that contained drag effects on the droplet and assumed a fast chemical reaction was suggested in [20–22]. Nonequilibrium models were proposed by Dushin et al. [23] and Tyurenkova [24] to consider the heating and cooling processes of droplets. They concluded that small droplets had longer lifetimes in the nonequilibrium condition due to evaporative cooling on the interface. As a result of Tyurenkova's result, droplet diameter in our study was on the order of approximately 100 μm, which was considered sufficient to ignore the nonequilibrium effect. Consequently, we adopted a simple Spalding method as Eqs. (10–14), and the estimated SMD could be used as the initial droplet diameter. Equation (10) indicates the flight distance of a liquid droplet through the hot burnt gas where Eqs. (12–14) are the internal variables in Eq. (10). Equation (12) indicates the drag on the droplets and Eq. (13) is the definition of transfer number using critical temperatures. Using the vaporization distance calculated from Eq. (10), vaporization time could be calculated by Eq. (14). Because the breakup length in the previous visualization study was short enough to be negligible in the vaporization calculation, it was assumed that the SMD of the droplet was the same as the initial droplet diameter and that there was no secondary breakup. The required chamber length and diameter could be determined by Eqs. (15) and (16) using the vaporization distance. The estimated spray angle should be applied in this procedure:

$$x^* = \left(\frac{D_{32}^2}{4}\right)\left[\frac{u_{d0}}{\sqrt{\gamma_c R_c T_c}} + \frac{3}{\Gamma}\left(\frac{A_t}{A_c}\right)\frac{S}{10}\right]\frac{c_{p,c}\rho_{\text{liq}}}{k_c}\frac{\sqrt{\gamma_c R_c T_c}}{\ell_n(1+B)}\frac{1}{(2+S)} \tag{10}$$

$$\Gamma = \left(\frac{\gamma+1}{2}\right)^{(\gamma+1)/2(\gamma-1)} \tag{11}$$

$$S = \frac{9}{2}\frac{Pr_c}{B} \tag{12}$$

$$B = \frac{T_c - T_{\text{cr}}}{T_{\text{cr}} - T_{\text{liq}}} \tag{13}$$

$$t^* = \frac{x^*}{\sqrt{\gamma_c R_c T_c}}\Gamma\left(\frac{A_c}{A_t}\right) \tag{14}$$

$$D_c = 2(x^*)\sin\alpha + D_{\text{pt}} \tag{15}$$

$$L_c = (x^*)\cos\alpha + L_{\text{open}} + r_{\text{post}} \tag{16}$$

The design method for a liquid rocket combustor proposed by Cho et al. [25] and Son et al. [26] was adopted to associate this design method with combustor performance analysis. The entire design procedure was established, as shown in Fig. 13. First, the design target was determined as the engine thrust, mixture ratio, chamber pressure, and throttling level of 100% based on the engine mission and combination of propellants. All combustion properties were calculated using a chemical equilibrium application [27] and all thermodynamic properties of the propellants were calculated from SUPERTRAPP [28], based on the principle of corresponding states. The subroutine for the pintle injector started after the mass flow rate calculation. The spray performances, including the spray angle and SMD, were calculated using the initial geometry. A feasibility check

Table 3 Example of target design

Parameter	Value
Thrust at 100% throttling, N	500
Chamber pressure at 100% throttling, MPa	2.0
Oxidizer (liquid)/fuel (gas)	LOx/GCH4
O/F ratio	4.0
Oxidizer injection temperature, K	90.17
Fuel injection temperature, K	300

Table 4 Dimensions of baseline pintle injector

Parameter	Value
Pintle tip diameter, mm	8.0
Annular gap thickness, mm	1.0
Center gap diameter, mm	6.0
Pintle rod diameter, mm	3.0
Post recess length, mm	3.0
Pintle tip angle, deg	20
Pintle-opening distance at 100% throttling, mm	0.5

Table 5 Design results of the baseline pintle injector at 100% throttling level

Parameter	Value
Pintle injection velocity, m/s	8.83
Annular injection velocity, m/s	84.03
Weber number	1802.3
Estimated spray angle, deg	52.61
Estimated SMD, μm	33.93
Vaporization time, ms	8.83
Actual vaporization distance, mm	84.04
Estimated chamber diameter, mm	74.40
Estimated cylinder length, mm	29.88

Table 6 Cases for sensitivity analysis of the throttling levels

Throttling level, %	Decrease in pintle-opening distance, mm			
	Case 1	Case 2	Case 3	Case 4
100	0.50	0.50	0.50	0.50
80	0.50	0.45	0.40	0.25
60	0.50	0.40	0.30	0.125
40	0.50	0.35	0.20	0.0625
20	0.50	0.30	0.10	0.03125

was conducted for the initial results of the chamber diameter and length. There were some important checkpoints in this process. First, the minimum area of the pintle nozzle had to be lower than the center gap area, as mentioned in the previous section. Additionally, injection velocities needed to be lower than the speed of sound and additional restrictions on velocities had to be considered from the hot firing test to avoid a blowout. Furthermore, because an excessive vaporization distance requires a large combustion chamber size, it should be controlled within a reasonable range. Moreover, the calculated chamber diameter should be larger than the injector module diameter. The iterative calculation began with the decrease in the throttling level down to its minimum value if all results were feasible. Then, the chamber diameter and length data could be obtained at all throttling levels. The maximum values could be chosen to cover all throttling levels from these databases.

B. Design Results

The sample design was applied to a 500 N thrust combustor with 5:1 throttling performance, as shown in Table 3 using the design procedure outlined previously. The target chamber pressure at the 100% throttling level was 2.0 MPa. The propellants were a combination of liquid oxygen and gaseous methane, and it was assumed that liquid oxygen was injected at the central pintle nozzle. The initial geometry was assumed to be similar to the experimental model shown in Table 4. The result shown in Table 5 was reasonable for this geometry. The maximum injection velocity was lower than the speed of sound, and the orders of injection velocities were feasible in terms of the performances of actual engines [29]. The effects of the throttling level upon the spray performances and chamber geometries were analyzed for the cases in Table 6 using this baseline. The opening distance was fixed at 0.5 mm for case 1. This distance decreased by 10, 20, and 50% of the previous values for cases 2–4, respectively.

Consequently, the spray angle was completely dependent upon the throttling level, regardless of the change in the opening distance, as shown in Fig. 14a, because the characteristic number defined by Eq. (5)

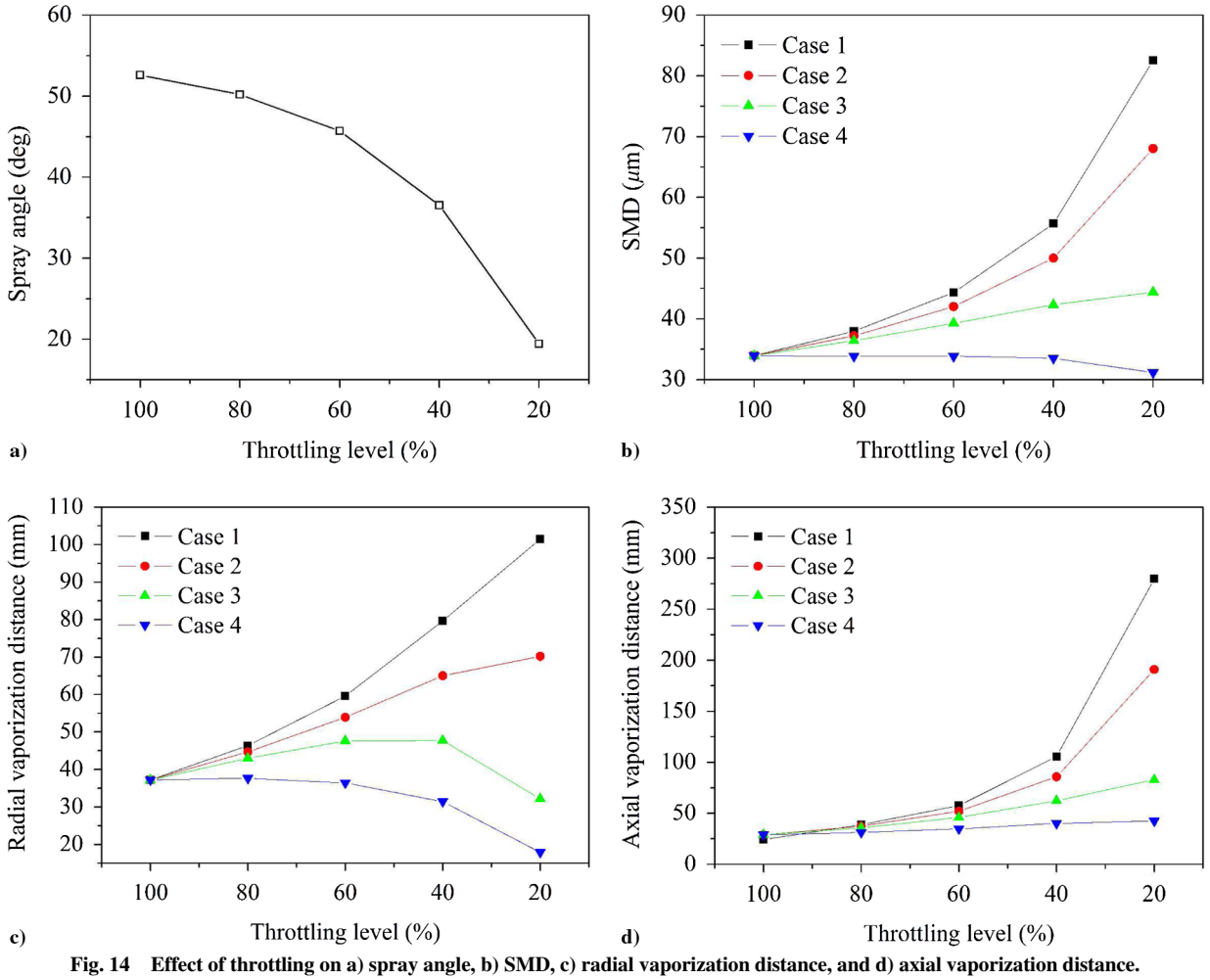

Fig. 14 Effect of throttling on a) spray angle, b) SMD, c) radial vaporization distance, and d) axial vaporization distance.

Table 7 Summary of designed combustor with 5:1 throttling performance

	100% throttling level	60% throttling level	20% throttling level
Thrust, N	500	300	100
Chamber pressure, MPa	2.0	1.2	0.4
Pintle tip diameter, mm	— —	8.0	— —
Annular gap thickness, mm	— —	1.0	— —
Center gap diameter, mm	— —	6.0	— —
Pintle rod diameter, mm	— —	3.0	— —
Post recess length, mm	— —	3.0	— —
Pintle tip thickness, mm	— —	1.0	— —
Pintle tip angle, deg	— —	20	— —
Pintle-opening distance, mm	0.5	0.3	0.1
Total mass flow rate, kg/s	0.159	0.096	0.032
Oxidizer mass flow rate, kg/s	0.128	0.077	0.026
Fuel mass flow rate, kg/s	0.032	0.019	0.006
Pintle injection velocity, m/s	8.83	8.88	8.99
Annular injection velocity, m/s	84.03	85.66	87.75
Weber number	1802.3	666.6	76.9
Estimated spray angle, deg	52.61	45.71	19.43
Estimated SMD, μm	33.93	39.28	44.40
Vaporization time, ms	1.870	0.433	0.612
Actual vaporization distance, mm	41.79	60.96	84.68
Radial vaporization distance, mm	33.20	43.64	28.17
Axial vaporization distance, mm	25.38	42.57	79.85

had no effect on the opening distance when the O/F ratio was fixed at a constant value for the best performance. This means that avoiding a reduction in the spray angle is impossible. Conversely, significant changes were observed for the other parameters. As shown in Fig. 14b, the SMD increased as throttling level decreased in all cases except case 4. This trend means that the engine will have poorer combustion performance at the lower throttling level due to the increase of SMD if there is no proper control of the opening distance. In a manner similar to the SMD trend, the radial and axial vaporization distances drastically monotonically increased for cases 1 and 2, whereas the diameter in case 3 decreased over the throttling level of 60%, as shown in Figs. 14c and 14d. In particular, a large increase in the vaporization distance was observed in case 1 without controlling the pintle, and this indicated the importance of applying the variable injector to the deep throttling application. These results also suggested that a control plan for the opening distance in case 4 was the optimal means to maintain high performance in the design of a small combustor. However, the opening distance at the 20% throttling level in case 4 was approximately 0.03 mm. There was a nonuniform injection problem below 0.1 mm of the opening distance in the spray experiment. Thus, this condition was not feasible and case 3 was chosen as the next best condition. This trend was used to obtain the chamber diameter and length to complete vaporization in the chamber.

In case 3, using Eqs. (15) and (16), the required maximum chamber diameter was calculated as 95.50 mm at a 40% throttling level and the required maximum chamber length was calculated as 83.35 mm at a 20% throttling level. These dimensions of the chamber geometry were used to design a combustor, and the results of the combustor design are summarized in Table 7. The decrease in the throttling level led to the proportional reduction in the chamber pressures and mass flow rates, and the opening distance was controlled by the case 3 plan. A combustor profile was designed by the modified Rao method for a large contraction ratio, as shown in Fig. 15. The estimated spray trajectories are also presented in Fig. 15 and were calculated by the vaporization distances in Table 7. As expected, the widest spray at the 60% throttling level was limited by the chamber diameter and the longest spray at a 20% throttling level was restricted by the cylindrical chamber length. These results indicate that the design procedure was feasible and well established.

Moreover, a sensitivity analysis was conducted for the baseline design at a 100% throttling level, as shown in Fig. 16. This sensitivity analysis indicated which design parameter most significantly affected performance. From the result of the sensitivity analysis, the need for precision manufacturing could be clearly understood. The variation of the opening distance was totally independent of the spray angle, whereas the pintle tip angle strongly influenced the spray angle, as shown in Fig. 16a. In addition, spray angles could be wider than the design point as the O/F ratio and chamber pressure increased. This result indicates that spray could strongly fluctuate under oscillation of the propellant supply. If spray fluctuation was coupled with heat release, combustion instability in the radial direction could occur. As shown in Fig. 16b, the SMD was not much affected by the pintle tip angle and opening distance, whereas other variances have proportional relations. Because the SMD determines the burning time and flight length of a droplet, oscillation of the O/F ratio and chamber pressure can cause longitudinal instability. As shown in Figs. 16c and 16d, annular tip thickness had the most critical effect on vaporization length. An increase in the radial vaporization distance is crucial to the wall-cooling problem. If nonvaporized oxygen droplets impact the combustor wall, the wall material can be rapidly oxidized and critically damaged. To avoid burning the combustor wall, the annular gap thickness and tip diameter should have negative tolerances when they are manufactured. In addition, too short control of the oxygen mass flow rate can lead to overshooting of the O/F ratio. Therefore, the control system of the pintle injector should be designed to avoid overshoot of the mass flow rate. Additionally, some control and restriction of manufacturing processes are required to burn all propellant inside the chamber, as shown in Fig. 16d. If the axial vaporization distance increases, unburnt propellant can be exhausted and there can be a loss of thrust.

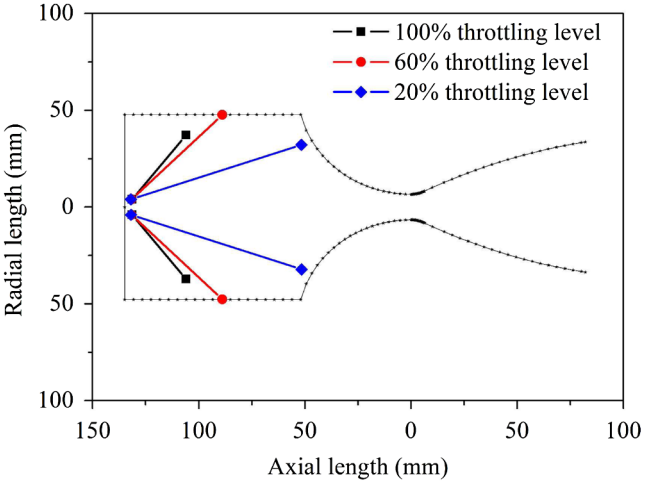

Fig. 15 Designed combustor profile and estimated spray trajectory according to throttling level.

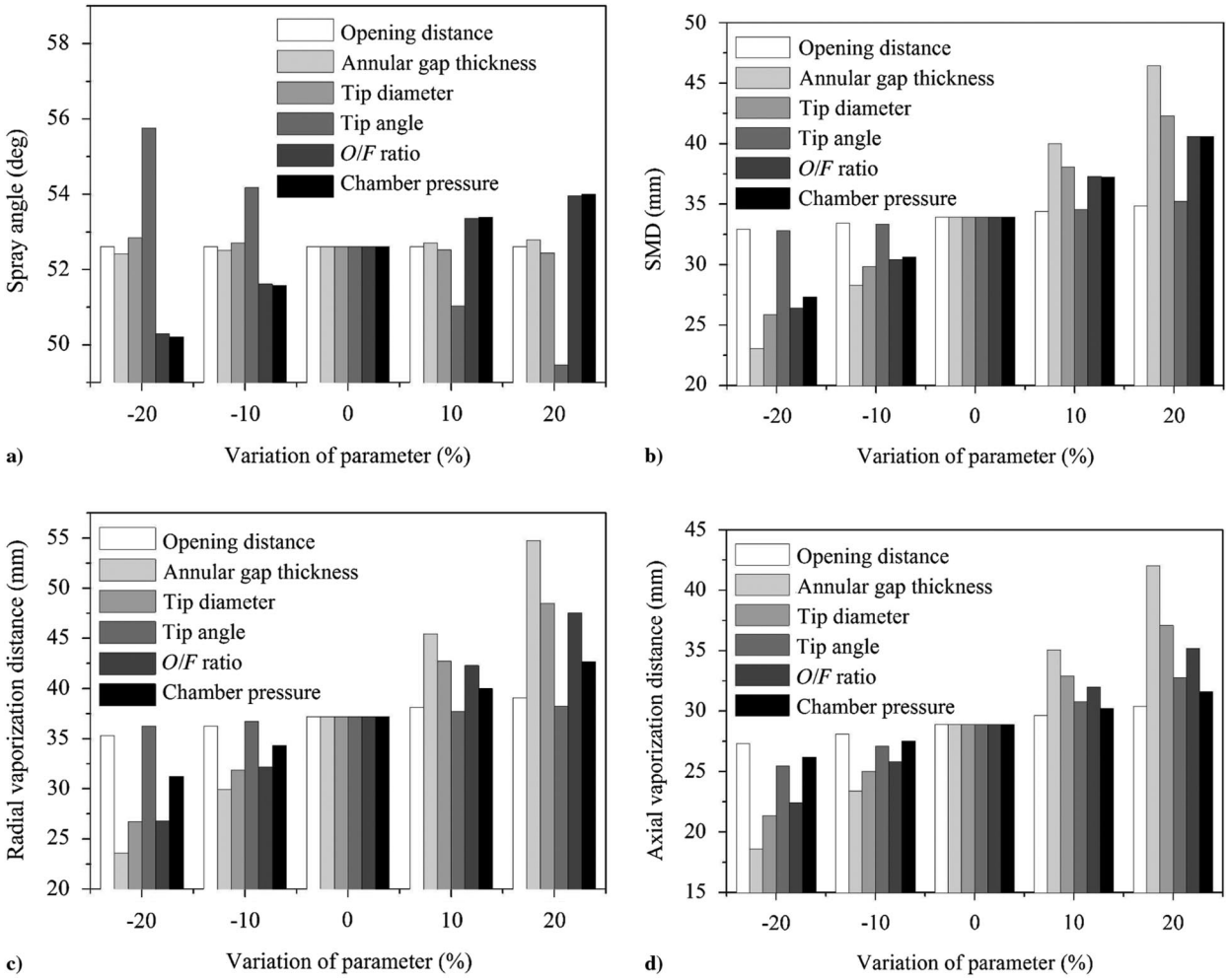

Fig. 16 Sensitivity of geometry variation on a) spray angle, b) SMD, c) radial vaporization distance, and d) axial vaporization distance.

IV. Conclusions

This study involved the development of an appropriate design procedure for a liquid–gas pintle injector for liquid rocket engines based on spray characteristics. The spray angle and Sauter mean diameter (SMD) were selected as the major performance parameters in an atmospheric experiment. Nondimensional numbers such as the velocity ratio, characteristic length, and Weber number were adopted to generalize the design procedure. The correlations needed to estimate the spray angle and SMD from the injector design were proposed using nondimensional numbers. The estimated spray angle and SMD were applied to restrict the diameter and length of the combustion chamber using a droplet vaporization model. This procedure for the pintle-injector analysis was merged with the combustor design method to establish an integrated design procedure. As a sample case, the procedure was used to design a pintle injector for a 500 N combustor with 5:1 throttleable performance. Four cases were examined to determine the pintle-opening distances at lower throttling levels, and the investigations revealed that it was feasible to decrease the pintle-opening distances in the same proportion as the throttling level. The results indicated that the geometries were reasonably designed and optimal performances were achieved for 60 and 20% throttling conditions. Avoiding reduction of the spray angle according to a decrease in the throttling level in sensitivity analysis was impossible, even though the pintle-opening distance changed. An effective method of changing the spray angle involved changing the pintle tip angle. The annular gap thickness was the most sensitive parameter for the SMD and chamber design. Hence, the results of this study revealed the major design parameters of a movable pintle injector and established a design procedure. Future research could investigate the application of the hot firing database to the design procedure and study its practical application to the design of a variable-thrust engine for several missions.

Acknowledgments

This work was supported by Advanced Research Center Program (NRF-2013R1A5A1073861) through the National Research Foundation of Korea grant funded by the Korea government contracted through Advanced Space Propulsion Research Center at Seoul National University.

References

[1] Casiano, M. J., Hulka, J. R., and Yang, V., "Liquid-Propellant Rocket Engine Throttling: A Comprehensive Review," *Journal of Propulsion and Power*, Vol. 26, No. 5, 2010, pp. 897–923. doi:10.2514/1.49791

[2] Gilroy, R., and Sackheim, R., "The Lunar Module Descent Engine-A Historical Summary," AIAA Paper 1989-2385, 1989. doi:10.2514/6.1989-2385

[3] Betts, E. M., and Frederick, R. A., Jr., "A Historical Systems Study of Liquid Rocket Engine Throttling Capabilities," AIAA Paper 2010-6541, 2010. doi:10.2514/6.2010-6541

[4] Dressler, G. A., and Bauer, J. M., "TRW Pintle Engine Heritage and Performance Characteristics," AIAA Paper 2000-3871, 2000. doi:10.2514/6.2000-3871

[5] Gavitt, K. R., and Mueller, T. J., "Testing of the 650 klbf LOX/LH2 Low Cost Pintle Engine," AIAA Paper 2001-3987, 2001. doi:10.2514/6.2001-3987

[6] Calvignac, J., Dang, L., Tramel, T. L., and Paseur, L., "Design and Testing of Non-Toxic RCS Thrusters for Second Generation Reusable

Launch Vehicle," AIAA Paper 2003-4922, 2003.
doi:10.2514/6.2003-4922
[7] Gromski, J. M., Majamaki, A. N., Chianese, S. G., Weinstock, V. D., and Kim, T. S., "Northrop Grumman TR202 LOX/LH2 Deep Throttling Engine Technology Project Status," AIAA Paper 2010-6725, 2010.
doi:10.2514/6.2010-6725
[8] Seedhouse, E., *Space X: Making Commercial Spaceflight a Reality*, Springer–Verlag, New York, 2013, pp. 156–165.
[9] Austin, B. L., and Heister, S. D., "Characterization of Pintle Engine Performance for Nontoxic Hypergolic Bipropellants," *Journal of Propulsion and Power*, Vol. 21, No. 4, 2005, pp. 627–635.
doi:10.2514/1.7988
[10] Bedard, M. J., Feldman, T. W., Rettenmaier, A., and Anderson, W., "Student Design/Build/Test of a Throttleable LOX-LCH4 Thrust Chamber," AIAA Paper 2012-3883, 2012.
doi:10.2514/6.2012-3883
[11] Yue, C. G., Chang, X. L., Yang, S. J., and Zhang, Y. H., "Numerical Simulation of a Pintle Variable Thrust Rocket Engine," *Communications in Computer and Information Science*, Vol. 159, July 2011, pp. 477–481.
doi:10.1007/978-3-642-22691-5
[12] Sakaki, K., Kakudo, H., Nakaya, S., Tsue, M., Isochi, H., Suzuki, K., Makino, K., and Hiraiwa, T., "Optical Measurements of Ethanol/Liquid Oxygen Rocket Engine Combustor with Planar Pintle Injector," AIAA Paper 2015-3845, 2015.
doi:10.2514/6.2015-3845
[13] Sakaki, K., Kakudo, H., Nakaya, S., Tsue, M., Kanai, R., Suzuki, K., Inagawa, T., and Hiraiwa, T., "Performance Evaluation of Rocket Engine Combustors Using Ethanol/Liquid Oxygen Pintle Injector," AIAA Paper 2016-5080, 2016.
doi:10.2514/6.2016-5080
[14] Son, M., Yu, K., Koo, J., Kwon, O. C., and Kim, J. S., "Effects of Momentum Ratio and Weber Number on Spray Half Angles of Liquid Controlled Pintle Injector," *Journal of Thermal Science*, Vol. 24, No. 1, 2015, pp. 37–43.
doi:10.1007/s11630-015-0753-7
[15] Son, M., Yu, K., Koo, K., Kwon, O., and Kim, J., "Injection Condition Effects of a Pintle Injector for Liquid Rocket Engines on Atomization Performances," *Journal of ILASS-Korea*, Vol. 20, No. 2, 2015, pp. 114–120.
doi:10.15435/JILASSKR.2015.20.2.114
[16] Yu, K., Son, M., and Koo, J., "Effects of Opening Distance on Liquid-Gas Spray of Pintle Injector Under Atmospheric Condition," *Journal of the Korean Society for Aeronautical and Space Sciences*, Vol. 43, No. 7, 2015, pp. 585–592.
doi:10.5139/JKSAS.2015.43.7.585
[17] Brock, J. R., and Bird, R. B., "Surface Tension and the Principle of Corresponding States," *AIChE Journal*, Vol. 1, No. 2, 1955, pp. 174–177.
doi:10.1002/(ISSN)1547-5905
[18] Li, W., Bi, S., Zhao, G., and Wu, J., "An Improved Prediction Equation of Refrigerants Surface Tension Based on the Principle of Corresponding States," *Chemical Research in Chinese Universities*, Vol. 30, No. 4, 2014, pp. 681–684.
doi:10.1007/s40242-014-3487-2
[19] Mishra, S. K., and Tripathi, S. N., "Evaluation of Excess Surface Tension of Ternary Liquid Mixture of Hexane, Decane, Hexadecane Using Brock and Bird's Relation at 303.16 K Temperature," *Oriental Journal of Chemistry*, Vol. 25, No. 1, 2009, pp. 249–252.
[20] Spalding, D. B., and Adler, J., "A One-Dimensional Theory of Liquid-Fuel Rocket Combustion," Her Majesty's Stationery Office, Aeronautical Research Council Technical Rept., London, 1960.
[21] Hill, P., and Peterson, C., *Mechanics and Thermodynamics of Propulsion*, 2nd ed., Addison Wesley, Reading, MA, 1992, pp. 584–587.
[22] Son, M., Koo, J., Cho, W. K., and Lee, E. S., "Conceptual Design for a Kerosene Fuel-Rich Gas-Generator of a Turbopump-Fed Liquid Rocket Engine," *Journal of Thermal Science*, Vol. 21, No. 5, 2012, pp. 428–434.
doi:10.1007/s11630-012-0564-z
[23] Dushin, V. R., Kulchitskiy, A. V., Nerchenko, V. A., Nikitin, V. F., Osadchaya, E. S., Phylippov, Y. G., and Smirnov, N. N., "Mathematical Simulation for Non-Equilibrium Droplet Evaporation," *Acta Astronautica*, Vol. 63, Nos. 11–12, 2008, pp. 1360–1371.
doi:10.1016/j.actaastro.2008.05.021
[24] Tyurenkova, V. V., "Non-Equilibrium Diffusion Combustion of a Fuel Droplet," *Acta Astronautica*, Vol. 75, June–July 2012, pp. 78–84.
doi:10.1016/j.actaastro.2012.01.010
[25] Cho, W. K., Seol, W. S., Son, M., Seo, M. K., and Koo, J., "Development of Preliminary Design Program for Combustor of Regenerative Cooled Liquid Rocket Engine," *Journal of Thermal Science*, Vol. 20, No. 5, 2011, pp. 467–473.
doi:10.1007/s11630-011-0497-y
[26] Son, M., Ko, S., and Koo, J., "Genetic Algorithm to Optimize the Design of Main Combustor and Gas Generator in Liquid Rocket Engines," *Journal of Thermal Science*, Vol. 23, No. 3, 2014, pp. 259–268.
doi:10.1007/s11630-014-0704-8
[27] Gordon, S., and McBride, B. J., "Computer Program for Calculation Complex Chemical Equilibrium Compositions and Applications," NASA RP-1311, June 1996.
[28] Huber, M. L., *NIST Thermophysical Properties of Hydrocarbon Mixtures Database (SUPERTRAPP) Version 3.2 Users' Guide*, National Inst. of Standards and Technology, Gaithersburg, MD, 2003.
[29] Rahman, S., "A Review of Coaxial Gas/liquid Spray Experiments and Correlations," AIAA Paper 1994-2772, 1994.
doi:10.2514/6.1994-2772

A. K. Gupta
Associate Editor